THE JOURNAL OF PHYSICAL CHEMISTRY B
A JOURNAL OF THE AMERICAN CHEMICAL SOCIETY

pubs.acs.org/JPCB

Article

Intramolecular Relaxation Dynamics Mediated by Solvent−Solute Interactions of Substituted Fluorene Derivatives. Solute Structural Dependence

Briana A. Capistran, Stephen H. Yuwono, Mehdi Moemeni, Soham Maity, Aria Vahdani, Babak Borhan, James E. Jackson, Piotr Piecuch, Marcos Dantus, and G. J. Blanchard*

Cite This: *J. Phys. Chem. B* 2021, 125, 12486−12499

Read Online

ACCESS | Metrics & More | Article Recommendations | Supporting Information

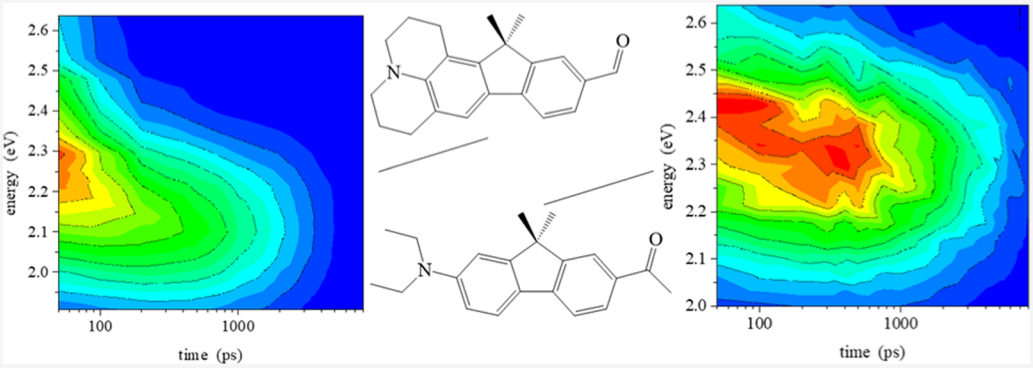

ABSTRACT: Several fluorene derivatives exhibit excited-state reactivity and relaxation dynamics that remain to be understood fully. We report here the spectral relaxation dynamics of two fluorene derivatives to evaluate the role of structural modification in the intramolecular relaxation dynamics and intermolecular interactions that characterize this family of chromophores. We have examined the time-resolved spectral relaxation dynamics of two compounds, NCy-**FR0** and MK-**FR0**, in protic and aprotic solvents using steady-state and time-resolved emission spectroscopy and quantum chemical computations. Both compounds exhibit spectral relaxation characteristics similar to those seen in **FR0**, indicating that hydrogen bonding interactions between the chromophore and solvent protons play a significant role in determining the relaxation pathways available to three excited electronic states.

INTRODUCTION

Photoactivated chemical reactants are a class of compounds with reactivities that can be controlled through light activation. These molecules become reactive only when in an excited electronic state, and this property is central to achieving high spatial and temporal control of chemical reactions. Applications such as precision chemistry and high-speed chemical sensing are enabled by this class of compounds. Prior to utilizing a photoactivated reagent in a chemical reaction, the relevant excited-state properties of the reagent must be understood at a level sufficient to provide insights into the reaction mechanism and potentially the reaction coordinate. In principle, photoreagents can be used to perform proton or electron exchange reactions, with proton exchange reactions being studied more extensively to date. The photoreagent for proton exchange reactions can function as a proton donor (photoacid)[1−17] or as a proton acceptor (photobase).[18−23] Photoacids are more numerous than photobases, and recent work has demonstrated a family of photobases capable of very large changes in basicity ($\Delta pK_b \sim 14$).[18−20]

The excited-state behavior of one of the few known superphotobases, **FR0**-SB (Figure 1a), has been characterized recently in protic and aprotic solvent environments, and the reaction coordinate and excited states have been identified for the solvent proton abstraction reaction.[18−20] In an effort to understand more fully the photoinduced change in reactivity of **FR0**-SB from a structural perspective, we have studied the excited-state relaxation dynamics of the aldehyde precursor, **FR0** (Figure 1b).[24] Using steady-state and time-resolved emission spectroscopy in conjunction with ab initio quantum chemistry calculations, multiple unresolved bands were found to contribute to the broad and relatively featureless steady-state emission spectrum of **FR0** in both protic and aprotic

Received: July 20, 2021
Revised: October 28, 2021
Published: November 9, 2021

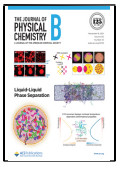

https://doi.org/10.1021/acs.jpcb.1c06475
J. Phys. Chem. B 2021, 125, 12486−12499

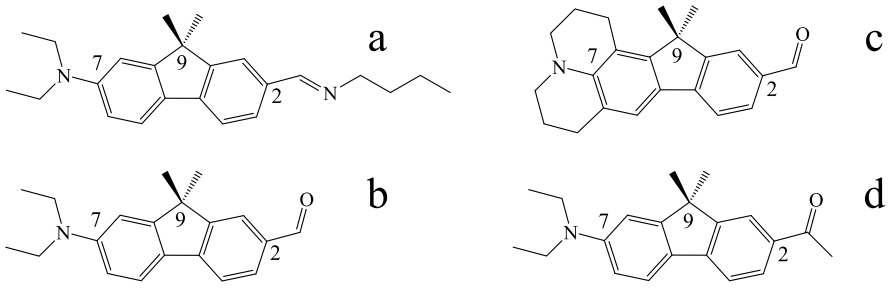

Figure 1. Molecular structures of (a) **FR0**-SB Schiff base, (b) **FR0** precursor, (c) NCy-**FR0** structural precursor, and (d) MK-**FR0** structural precursor.

Scheme 1. Synthesis of (a) NCy-FR0 and (b) MK-FR0

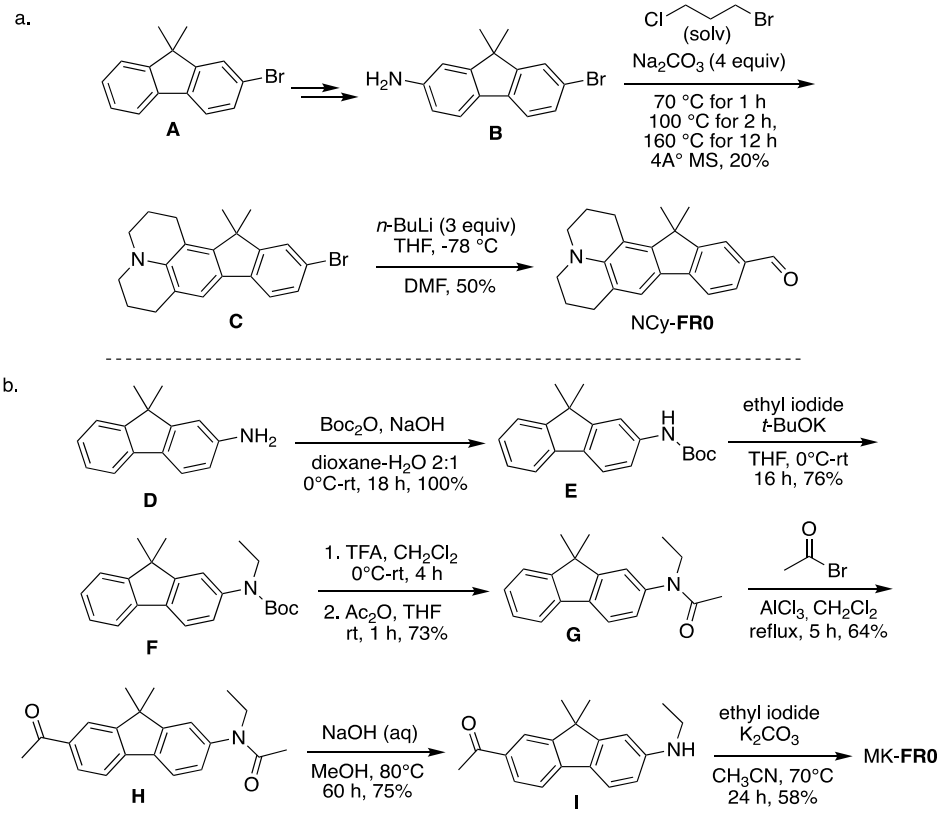

solvents. The individual bands were associated with three excited singlet electronic states in relatively close energetic proximity. The solvent medium was found to exhibit significant control over the coupling and relaxation rates between the electronic states in **FR0**. State-dependent relaxation dynamics were observed in protic solvents, whereas the coupling between electronic excited states was markedly different for **FR0** in dipolar aprotic solvents. The state-dependent relaxation dynamics of **FR0** in protic solvents were found to depend on solvent hydroxyl group concentration, analogous to the behavior seen for the super-photobase **FR0**-SB. For the **FR0** precursor, quantum chemical calculations demonstrated that the S_2 state exhibited a change in electron density distribution that is localized in the vicinity of the aldehyde moiety, which is significantly different from the electron density distributions for either the S_1 or S_3 states. This state-dependent variation in electron density distribution at the aldehyde gives rise to state-dependent differences in the permanent dipole moment, and we postulated that hydrogen bonding to **FR0** in its S_2 state mediated intramolecular relaxation pathways involving this electronic state. The site for the relevant hydrogen bond is the carbonyl oxygen, with the lone pairs on the oxygen presumably interacting with solvent hydroxyl protons.

The postulate that solvent hydrogen bonding interactions with the **FR0** aldehyde carbonyl moiety are primarily responsible for the observed spectral dynamics can be tested by making systematic structural changes to the **FR0** molecule and relating these changes to the spectral relaxation dynamics of the modified compounds. We report those studies here. Two **FR0** derivatives were examined, NCy-**FR0** (Figure 1c), possessing a cyclized amino functionality, and MK-**FR0** (Figure 1d), the methyl ketone analogue of the **FR0** aldehyde. These structural modifications were targeted because of their ability to address two specific issues. The first issue, whether or not the charge-transfer excited state(s) contributes to the observed spectral relaxation dynamics, can be evaluated by restricting the rotational freedom of the **FR0** amino group. The cyclization of the amino functionality of **FR0** and comparison

https://doi.org/10.1021/acs.jpcb.1c06475
J. Phys. Chem. B 2021, 125, 12486−12499

of the spectral relaxation dynamics of the free and cyclized species address this issue directly. The second issue is the role of the aldehydic proton in the observed spectral dynamics. Replacement of the aldehydic proton with a methyl group to form the methyl ketone affords a direct examination of the role of the carbonyl moiety. The data reported here reveal the absence of contributions from charge-transfer excited states to the observed spectral dynamics. Subtle differences are seen in the spectral dynamics of the aldehyde and ketone. While both compounds undergo hydrogen bonding with protic solvents, the differences in the electron density distributions of the aldehyde and ketone moieties lead to differences in dipolar contributions to the observed dynamics.

EXPERIMENTAL AND COMPUTATIONAL DETAILS

Materials. *n*-Propanol (99.7%, anhydrous) and dimethyl sulfoxide (DMSO, ≥99.9%, anhydrous) were purchased from Sigma-Aldrich and used as received. All chemicals and solvents were purchased from Sigma-Aldrich and used without further purification. Syntheses of NCy-**FR0** and MK-**FR0** are depicted in Scheme 1a,b, respectively.

C: Scheme 1a depicts the synthesis of NCy-**FR0** starting from the known 9,9-dimethylated monobromo fluorene **A**.[25] The bromo amine **B** (200 mg, 0.7 mmol, 1 equiv), 1-bromo-3-chloropropane (0.6 mL), Na_2CO_3 (297 mg, 2.8 mmol, 4 equiv), and 4 Å MS (50 mg) were added to a 50 mL flask and heated with vigorous stirring under an argon atmosphere by a gradual increase in temperature (70 °C for 1 h, 100 °C for 2 h, and 160 °C for 12 h). The resulting mixture was then cooled to room temperature, the excess 1-bromo-3-chloropropane was distilled off, and the residue was picked up in CH_2Cl_2. The crude solution in dichloromethane was extracted with water two times and dried with anhydrous sodium sulfate, and the solvent of the combined organics was removed under reduced pressure. The residue was washed with hot MeOH three times, and the product, obtained as a brown solid (50 mg, 0.14 mmol, 20%), was used in the next step.

^{1}H NMR (500 MHz, $CDCl_3$): δ 7.40 (s, 1H), 7.33 (m, 2H), 7.15 (s, 1H), 3.20 (q, J = 6.5 Hz, 4H), 3.01 (t, J = 6.4 Hz, 2H), 2.83 (t, J = 6.5 Hz, 2H), 2.01 (dt, J = 18.1, 6.1 Hz, 4H), 1.55 (s, 6H). ^{13}C NMR (126 MHz, $CDCl_3$): δ 155.67, 148.01, 143.19, 138.87, 129.73, 126.73, 125.26, 120.80, 119.28, 118.73, 118.50, 118.27, 50.79, 50.08, 48.21, 28.43, 25.12, 24.35, 22.12, 21.89.

NCy-**FR0**: The bromo fluorene **C** (500 mg, 1.4 mmol, 1 equiv) was dissolved in dry THF (30 mL), and the solution was cooled down to −78 °C under an argon atmosphere. *n*-Buli (2.5 M in hexane, 1.7 mL) was added to the resulting solution dropwise and stirred for 45 min. Formylation of the resulting metal−halogen exchanged intermediate was achieved by addition of dry DMF (2.7 mL, 25 equiv), which was stirred for 2 h at −78 °C and at room temperature for another 12 h. The reaction was quenched with water (10 mL) and extracted with ethyl acetate three times; the combined organics were dried with sodium sulfate, and the solvent was removed under reduced pressure. The resulting crude was washed with hot MeOH three times and dried to get the pure compound as a yellow fluorescent solid (222 mg, 0.7 mmol, 50%).

^{1}H NMR (500 MHz, $CDCl_3$): δ: 9.95 (s, 1H), 7.81 (d, J = 1.0 Hz, 1H), 7.73 (dd, J = 8 Hz, 1.5 Hz, 1H), 7.56 (d, J = 7.9 Hz, 1H), 7.25 (s, 1H), 3.22−3.26 (m, 4H), 3.03 (t, J = 6.4 Hz, 2H), 2.84 (t, J = 6.5 Hz, 2H), 2.10−1.88 (m, 4H), 1.59 (s, 6H). ^{13}C NMR (126 MHz, $CDCl_3$): δ: 192.01, 154.03, 150.13, 146.78, 144.29, 131.16, 126.99, 125.76, 122.00, 120.95, 119.97, 118.13, 117.67, 50.69, 50.00, 47.86, 28.43, 24.94, 24.24, 21.87, 21.62.

E: The synthesis of MK-**FR0** is depicted in Scheme 1b. A solution of 9,9-dimethyl-9*H*-fluoren-2-amine **D**, (1 equiv, 4.77 mmol, 1.0 g) dissolved in a mixture of dioxane−H_2O (2:1) and 2 N NaOH (0.6 mL) was cooled to 0 °C. Boc_2O (1.75 equiv, 1.21 mmol, 0.265 g) was added in one portion, and the mixture was stirred while warming to room temperature, for 18 h. The reaction was quenched by acidifying the solution with 1 M $KHSO_4$ (0.5 mL) to pH 3, which yielded the product as a precipitate. The precipitated solid was then washed with ice-cold water (3 mL), dioxane−H_2O (2:1, 5 mL) and hexanes (5 mL) and was subsequently dried overnight in the presence of P_2O_5 to yield a yellow-white solid (0.99 g, 100%). The product was used without further purification in the next step.

^{1}H NMR (500 MHz, $CDCl_3$): 1.48 (s, 6 H), 1.55 (s, 9H), 6.54 (bs, 1H), 7.19 (dd, J = 8.2, 2.0 Hz, 1H), 7.32 (td, J = 7.4, 1.3 Hz, 1H), 7.43−7.40 (m, 1H), 7.67−7.61 (m, 3H).

F: To an ice-cold mixture of *tert*-butyl (9,9-dimethyl-9*H*-fluoren-2-yl)carbamate **E** (1 equiv, 3.23 mmol, 1 equiv) and ethyl iodide (2.5 equiv, 8.07 mmol, 0.65 mL) dissolved in dry THF (25 mL) was added potassium *tert*-butoxide (4 equiv, 12.9 mmol, 1.5 g) in three portions over 30 min. The resultant mixture was stirred overnight for 16 h. After this time, H_2O (15 mL) was added, and the mixture was extracted with CH_2Cl_2 (3 × 10 mL) and dried over anhydrous magnesium sulfate, and the solvent was removed under reduced pressure. The resulting crude compound was purified using flash chromatography (0 → 12% EtOAc in hexanes) to yield the pure product as a pale-yellow oil (0.82 g, 76%).

^{1}H NMR (500 MHz, $CDCl_3$): δ 1.20 (t, J = 7.1 Hz, 3H), 1.44 (s, 9H), 1.49 (s, 6H), 3.73 (q, J = 7.1 Hz, 2H), 7.16 (d, J = 7.5 Hz, 1H), 7.23 (s, 1H), 7.30−7.37 (m, 2H), 7.42−7.45 (m, 1H) 7.66 (d, J = 8.0 Hz, 1H), 7.69−7.72 (m, 1H).

G: A solution of *tert*-butyl (9,9-dimethyl-9*H*-fluoren-2-yl)(ethyl)carbamate **F** (1 equiv, 0.723 mmol, 0.244 g) in dry CH_2Cl_2 (6 mL) was cooled to 0 °C followed by the dropwise addition of trifluoroacetic acid (10 equiv, 7.23 mmol, 0.55 mL). The solution was stirred at this temperature for 30 min and was warmed to room temperature where it was stirred for an additional 4 h. The reaction was then quenched using saturated $NaHCO_3$ (10 mL), and the organic layer was separated. The aqueous layer was extracted with CH_2Cl_2 (3 × 10 mL), and the combined organics were dried over anhydrous sodium sulfate, and the solvent was removed under reduced pressure. The crude deprotected fluorene was used directly in the next step without any further purification. The intermediate was then redissolved in THF (5 mL) followed by addition of acetic anhydride (2 equiv, 1.45 mmol, 0.14 mL), and the mixture was stirred at ambient temperature for 1 h. The reaction was quenched with saturated $NaHCO_3$ (10 mL), followed by separation of the organic layer. The aqueous layer was extracted with CH_2Cl_2 (3 × 10 mL), and the combined organics were dried over anhydrous sodium sulfate, and the solvent was removed under reduced pressure. The crude acylated product was purified via flash chromatography (1:9 EtOAc/hexanes), yielding the pure compound **G** as a beige-yellow solid (0.148 g, 73%).

^{1}H NMR (500 MHz, $CDCl_3$): δ 1.18 (t, J = 7.2 Hz, 3H), 1.51 (s, 6H), 1.91 (s, 3H), 3.82 (t, J = 7.2 Hz, 2H), 7.13 (dd, J = 7.9, 1.9 Hz, 1H), 7.21 (d, J = 1.9 Hz, 1H), 7.35−7.39 (m, 2H), 7.38−7.45 (m, 1H), 7.72−7.77 (m, 2H).

https://doi.org/10.1021/acs.jpcb.1c06475
J. Phys. Chem. B 2021, 125, 12486−12499

H: To a solution of *N*-(9,9-dimethyl-9*H*-fluoren-2-yl)-*N*-ethylacetamide **G** (1 equiv, 0.49 mmol, 0.138 g) in dry CH_2Cl_2 (8 mL) under an atmosphere of argon was added aluminum chloride (3 equiv, 1.5 mmol, 0.20 g). The mixture was stirred for 5 min before the dropwise addition of acetyl bromide (1 equiv, 0.49 mmol, 0.036 mL). The mixture was stirred at 40 °C for 4 h, where at each hour, fresh portions of aluminum chloride (3 equiv, 1.5 mmol, 0.20 g) were added to the reaction. The mixture was quenched by the slow addition of $NaHCO_3$ (5 mL); the organic layer was separated, and the aqueous layer was extracted with CH_2Cl_2 (3 × 10 mL). The combined organic mixture was dried over anhydrous magnesium sulfate, and the solvent was removed under reduced pressure, yielding the crude compound. The crude was purified via flash chromatography (30 → 80% EtOAc in hexanes), yielding the product **H** as a pure white solid (0.101 g, 64%).

^{1}H NMR (500 MHz, $CDCl_3$): δ 1.19 (t, J = 7.1 Hz, 3H), 1.54 (s, 6H), 2.00 (s, 3H), 2.68 (s, 3H), 3.84 (q, J = 7.2 Hz, 2H), 7.15−7.20 (m, 1H), 7.25 (m, 1H), 7.79−7.84 (m, 2H), 7.99 (dd, J = 8.0, 1.6 Hz, 1H), 8.07 (d, J = 1.6 Hz, 1H).

I: To the solution of *N*-(7-acetyl-9,9-dimethyl-9*H*-fluoren-2-yl)-*N*-ethylacetamide **H** (1 equiv, 0.316 mmol, 0.102 g) dissolved in methanol (2 mL) was added 6 N NaOH (0.4 mL). The mixture was stirred at 80 °C for 60 h, before cooling it to room temperature. The reaction was diluted with water (5 mL) and extracted with CH_2Cl_2 (3 × 5 mL), and the combined organics were dried over anhydrous magnesium sulfate. The solvent was removed under reduced pressure, and the crude was purified via flash chromatography (5 → 25% EtOAc in hexanes) to yield pure compound **I** as a yellow solid (0.067 g, 75%).

^{1}H NMR (500 MHz, DMSO-d_6): δ 1.19 (t, J = 7.1 Hz, 3H), 1.40 (s, 6H), 2.57 (s, 3H), 3.06−3.17 (m, 1H), 5.99 (t, J = 5.2 Hz, 1H), 6.57 (dd, J = 8.3, 2.1 Hz, 1H), 6.69 (d, J = 2.2 Hz, 1H), 7.60 (d, J = 8.2 Hz, 1H), 7.65 (d, J = 8.0 Hz, 1H), 7.88 (dd, J = 7.8, 1.6 Hz, 1H), 7.87 (d, J = 1.6 Hz, 1H).

MK-**FR0**: Ethyl iodide (4 equiv, 0.356 mmol, 0.0915 mL) was added to a stirred solution of 1-(7-(ethylamino)-9,9-dimethyl-9*H*-fluoren-2-yl)ethan-1-one **I** (1 equiv, 0.089 mmol, 0.025 g) and K_2CO_3 (1.5 equiv, 0.134 mmol, 0.0184 g) in dry acetonitrile (1.0 mL). The mixture was stirred at 70 °C for 24 h, before quenching with the addition of H_2O (3 mL). The organic layer was then extracted with CH_2Cl_2 (3 × 2 mL), and the combined organics were dried over anhydrous magnesium sulfate. The solvent was removed under reduced pressure, followed by purification of the crude yellow solid by flash chromatography (5 → 20% EtOAc in hexanes) to yield the pure compound as a yellow solid (0.016 g, 58%).

^{1}H NMR (500 MHz, $CDCl_3$): 1.24 (t, J = 7.0 Hz, 6H), 1.49 (s, 6H), 2.64 (s, 3H), 3.46 (q, J = 7.1 Hz, 4H), 6.67−6.72 (m, 2H), 7.56−7.63 (m, 2H), 7.91 (dd J = 8.0, 1.6 Hz, 1H), 7.98 (d, J = 1.6 Hz, 1H).

Sample Preparation. Following synthesis, each compound was stored in ethanol at a concentration of 1 mM. The compounds were prepared for spectroscopic analysis following a procedure similar to that used for **FR0**. Briefly, each compound was brought to dryness with N_2(g) and reconstituted in the solvent system to be studied (*n*-propanol, DMSO, and a binary solvent mixture of *n*-propanol/DMSO). Sample concentrations were ca. 5 × 10^{-6} M for the spectroscopic measurements.

Steady-State Emission and Time-Resolved Fluorescence Spectroscopy. Collection of steady-state and time-resolved emission spectra was performed using the same instrumentation and parameters for analysis of **FR0**,[24] and the time-correlated single-photon counting (TCSPC) instrument has been described in detail elsewhere.[26] The time resolution of this instrument, determined by its instrument response function, is ca. 35 ps. Excitation of the samples was at 440 nm with 5 ps pulses. For time-domain TCSPC measurements, emission decays were acquired across the wavelength range of 470−620 nm, in 10 nm increments. The acquired time-domain polarized emission data components were exported to Microsoft Excel (Microsoft Office 365, Microsoft Corporation, Redmond, WA). Microcal Origin (OriginPro 9.0, OriginLab Corporation, Northampton, MA) was used for subsequent data processing and analysis, band fitting, and determination of fluorescence lifetime decay constants.

Summary of Computational Protocol. In addition to the abovementioned experiments, we report the results of quantum chemistry computations following the protocol described in ref 24. Thus, for each of the molecular species considered in this work, we calculated the vertical excitation energies corresponding to the four lowest singlet excited states using the composite procedure combining the equation-of-motion coupled-cluster approach with singles and doubles (EOMCCSD)[27] employing the 6-31+G* basis set[28−30] with the triple corrections of the δ-CR-EOMCC(2,3) method of refs 313233 and the 6-31G basis.[30] We also computed dipole moments, transition dipole moments, oscillator strengths, Mulliken charges, and electron densities characterizing the ground and four lowest singlet excited states using the EOMCCSD/6-31+G* approach. In ref 24, all calculations were performed using the GAMESS package.[34,35]

RESULTS AND DISCUSSION

To investigate the effects of structural changes to the **FR0** molecule on spectral dynamics, spectroscopic fluorescence lifetime measurements were performed for NCy-**FR0** and MK-**FR0** in *n*-propanol and DMSO to represent the same protic and aprotic media used in the analysis of **FR0**. The results of quantum chemical calculations for NCy-**FR0** and MK-**FR0** were used in conjunction with the time-resolved emission data to gain insights into the structure dependence of the relaxation dynamics. We have studied the spectral dynamics of NCy-**FR0** to evaluate the role of large amplitude motion. For NCy-**FR0**, the diethyl amino group on **FR0** is tethered to the fluorene ring system (Figure 1c), preventing rotation about the ring carbon to the amino nitrogen bond. This structural modification prevents the amino nitrogen from participating in a twisted intramolecular charge-transfer state.

Table 1. $S_0 \rightarrow S_n$ Vertical Excitation Energies $\omega_n^{(EOMCC)}$ and the Permanent Dipole Moments μ_n Characterizing the Lowest Four Excited Singlet States of NCy-FR0 in the Gas Phase[a]

state	$\omega_n^{(EOMCC)}$ (eV)	μ_n (D)
S_1	3.46	14.4
S_2	3.82	2.2
S_3	3.80	8.9
S_4	4.15	4.3

[a]The dipole moment of NCy-**FR0** in the ground S_0 state is 6.0 D.

https://doi.org/10.1021/acs.jpcb.1c06475
J. Phys. Chem. B 2021, 125, 12486−12499

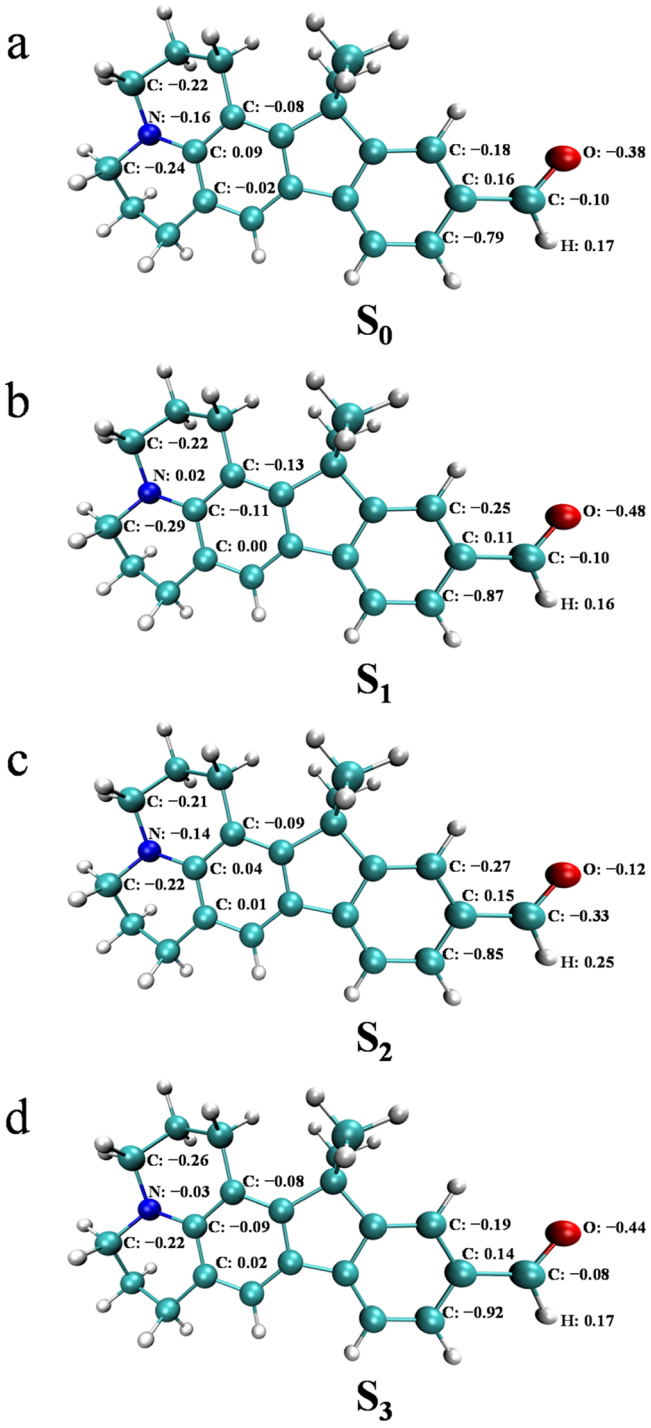

Figure 2. Structure of the isolated NCy-**FR0** chromophore in its ground electronic S_0 state and the computed Mulliken charges for selected atoms in (a) S_0, (b) S_1, (c) S_2, and (d) S_3 states of NCy-**FR0**.

Our quantum chemical calculations for NCy-**FR0** show three excited singlet states in close energetic proximity (Table 1), similar to **FR0**. The energetic proximity of these three states is consistent with facile relaxation between S_3, S_2, and S_1. Note that the computed vertical excitation energies characterizing the $S_0 \rightarrow S_2$ and $S_0 \rightarrow S_3$ transitions differ by only 0.02 eV, which is within the uncertainty range of our computational protocol. Thus, we also examined other properties associated with the S_2 and S_3 states of NCy-**FR0**, such as the permanent and transition dipole moments, and compared them with those

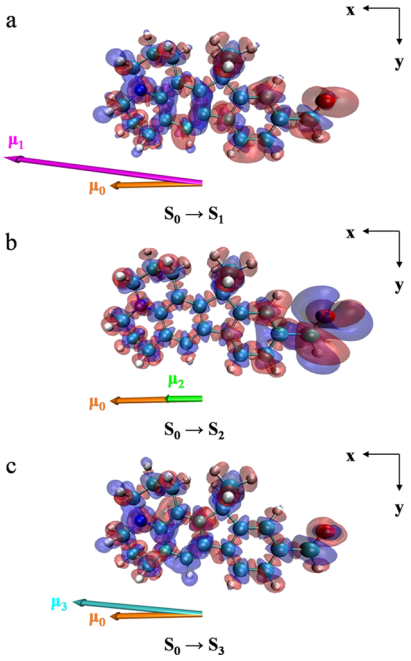

Figure 3. Structure of the isolated NCy-**FR0** molecule in its ground electronic S_0 state and the electronic density difference maps associated with the vertical transitions from S_0 to (a) S_1, (b) S_2, and (c) S_3 states of NCy-**FR0**. The red/blue color indicates an increase/decrease in electron density upon the $S_0 \rightarrow S_n$ (n = 1−3) excitation, respectively. The dipole moment vectors characterizing the S_0 (orange), S_1 (magenta), S_2 (green), and S_3 (cyan) states of NCy-**FR0** are shown as well.

reported in ref 24 for the **FR0** precursor molecule to determine the state ordering shown in Table 1. Our calculations indicate that the permanent dipole moment of NCy-**FR0** in its S_2 singlet excited state is noticeably smaller than that characterizing the remaining excited states listed in Table 1. In analogy to **FR0**, solvent−solute interactions in the S_2 state appear to play a substantial role in mediating intramolecular relaxation dynamics for NCy-**FR0**. The transition dipole moments and oscillator strengths characterizing vertical excitations in NCy-**FR0** are similar to those obtained for **FR0** in ref 24 and presented in Table S1 in the Supporting Information.

The Mulliken charges for the aldehyde functionality, specifically the carbonyl group, in the S_2 state of NCy-**FR0** (Figure 2) are almost identical to those of **FR0** in the S_2 excited state.[24] The carbonyl oxygen exhibits a more positive charge in the S_2 state, with an effective charge of ca. −0.1, than in the S_1 and S_3 states, where the carbonyl oxygen carries ca. −0.4 effective charge (Figure 2). The state-dependent changes in the Mulliken charges of the aldehyde moiety are manifested as state-dependent changes in permanent dipole moments for each excited state (Table 1), shown visually, along with the corresponding S_n−S_0 electron density differences, in Figure 3. The Mulliken charge on the amino nitrogen atom is close to zero in the ground state and the excited states (Figure 2). There is no evidence from the computational data of any contribution from a charge-transfer species to the excited electronic states. Thus, the interactions between solvent protons and the amino nitrogen are expected to be modest, and no state dependence is expected. Not surprisingly, the results of our quantum chemical calculations for NCy-**FR0** are very similar to those obtained for **FR0**. Large-amplitude

https://doi.org/10.1021/acs.jpcb.1c06475
J. Phys. Chem. B 2021, 125, 12486−12499

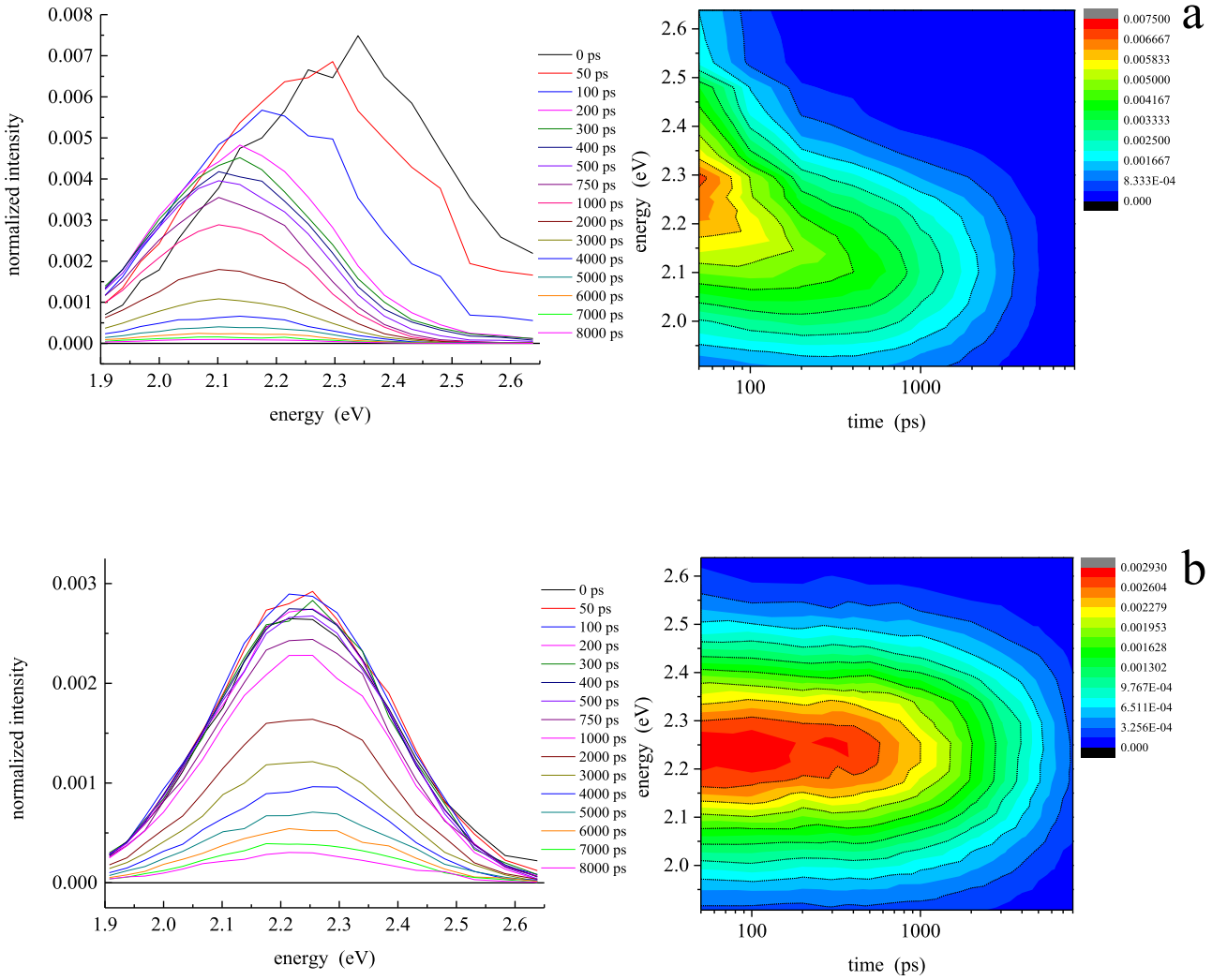

Figure 4. Time-resolved emission spectra for NCy-**FR0** in (a) *n*-propanol and (b) DMSO extracted from experimental fluorescence lifetime data. For the spectra in the left panels, the time corresponding to each spectrum is provided in the legends. The right panels are contour plots of the time-resolved spectra.

Table 2. Fitted Rate Constants for the Relaxations Associated with Each of the Three Fitted Emission Bands (Spectral Features) for NCy-FR0 in *n*-Propanol and DMSO

	solvent	
rate constant (Hz)	*n*-propanol ($\times 10^9$)	DMSO ($\times 10^9$)
k_{32}	9.21 ± 0.87	0.08 ± 0.03
k_{31}	4.93 ± 1.14	0.08 ± 0.07
k_{30}	8.26 ± 1.22	0.21 ± 0.08
k_{21}	0.52 ± 0.30	0.05 ± 0.02
k_{20}	1.46 ± 0.41	0.24 ± 0.02
k_{10}	0.65 ± 0.25	0.80 ± 0.14

rotational motion of the amino group is thus shown to not contribute to the spectral dynamics seen for the **FR0** chromophore.

Before proceeding to the discussion of our experimental results, it is important to consider at the outset how to interpret the time-resolved fluorescence data. Time-resolved spectral evolution of broad, relatively featureless emission bands has been reported previously, and the appropriate treatment of such data depends on information beyond the spectral shift alone. The central question is whether the time-resolved red shift of a broad emission spectrum could, in principle, be either due to the relaxation of a single electronic manifold along a coordinate mediated by the rate at which the surrounding medium relaxes[36−44] or due to intramolecular relaxation between unresolved electronic state manifolds within the molecule.[45−54] For most complex organic chromophores, it is likely that both intermolecular interactions and intramolecular relaxation contribute to the observed spectral dynamics. Quantum chemical computations can be of assistance in resolving the electronic structure of organic chromophores.[24,50,51] When multiple electronic states are shown to exist in close energetic proximity, intramolecular relaxation is expected to contribute to the observed spectral dynamics, although our quantum chemical computations cannot accurately predict the extent to which the intramolecular processes operate because such computations cannot account for intermolecular (solvent−solute) interactions at a level sufficient to model environmental mediation of the intramolecular relaxation processes.

We also recognize that it is unusual for higher excited singlet states to play a significant role in the radiative relaxation dynamics of an organic chromophore.[55,56] However, vibronic intensity borrowing can play a role in accounting for relaxation

https://doi.org/10.1021/acs.jpcb.1c06475
J. Phys. Chem. B 2021, 125, 12486−12499

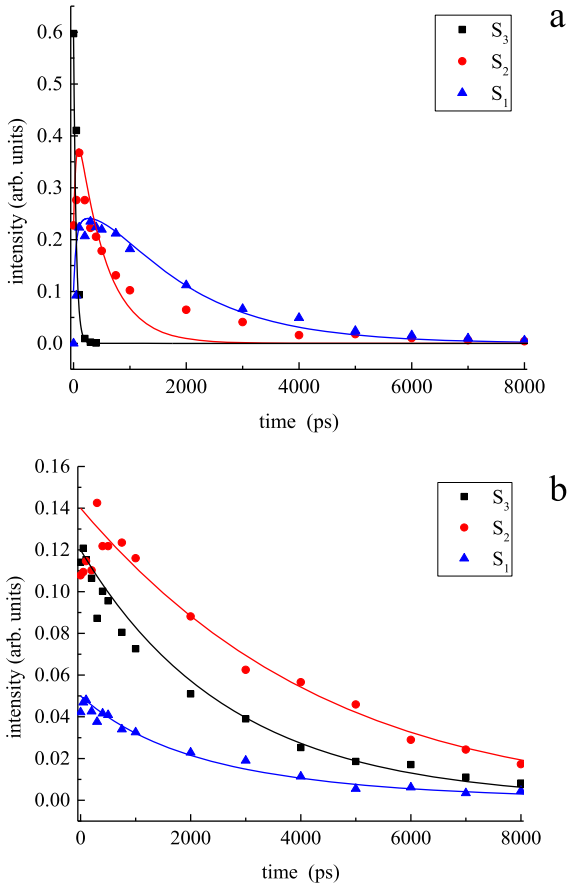

Figure 5. Time-dependent band intensities for three fitted emission bands for NCy-**FR0** in (a) *n*-propanol and (b) DMSO. The data are fitted to the kinetic model using the rate constants in Table 2.

dynamics between electronic states that are mediated by the properties of the local environment.[57−59] For the structurally modified **FR0** chromophores studied in this work, namely, NCy-**FR0** and MK-**FR0** (vide infra), there are several closely spaced electronic states, and this situation can give rise to substantial modification of the relative intensities of the absorption and emission bands when compared to results calculated assuming either a vacuum or continuum dielectric medium. Our findings for the unmodified **FR0** molecule shown in ref 24 are also consistent with vibronic intensity borrowing, accounting for the spectral dynamics that we observe.

The excited-state relaxation dynamics of NCy-**FR0** are consistent with the results of our quantum chemical calculations. Time-resolved fluorescence lifetime decays in *n*-propanol and DMSO were collected over a wavelength range (470−620 nm) and normalized to the steady-state fluorescence emission spectra collected for each solvent medium. The time-resolved spectra were generated from the experimental lifetime decays (Figures S1 and S2 in the Supporting Information) at various time points across the collection period as a function of emission wavelength (Figure 4). The results display a spectral shift (wavelength dependence) in protic media (Figure 4a), whereas the dynamics remain constant in aprotic media (Figure 4b).

To further investigate the observed spectral dynamics of NCy-**FR0**, the steady-state emission spectrum in each solvent was treated in the same way described for that of **FR0**[24] to identify the three Gaussian bands within the broad spectra (Figure S2 in the Supporting Information). The corresponding intensities of each fitted band within the extracted time-resolved spectra (Figure 4) were determined, and from these fits, we generate the time evolution of each band, which corresponds to the solvent−solute complex in each excited state. Consistent with the analysis of **FR0**, the highest-energy emission band was assigned to the $S_3 \rightarrow S_0$ emission, the intermediate band was assigned to $S_2 \rightarrow S_0$, and the lowest-energy band was assigned to the $S_1 \rightarrow S_0$ emission. Taking the resulting time-dependent band intensities, we applied a kinetic model[24] to determine the fitted rate constants associated with the relaxations in each state (i.e., the relaxation of each fitted emission band), which are presented in Table 2 and Figure 5. We present this model in the Supporting Information (Figure S3 and eqs S.1−S.6 in the Supporting Information). The determination of best-fit rate constants using this model does not provide unique rate constants because this is an inherently underdetermined problem. Nevertheless, it is possible to apply self-consistency across the datasets and enforce trivial limits such as positive values only for rate constants. With the abovementioned caveat, we present the fitted rate constant values in Table 2.

Several trends emerge from these fitted results. The relaxation dynamics of NCy-**FR0** in *n*-propanol appear to be qualitatively different from those in DMSO (Table 2). The fitted rate constants for NCy-**FR0** in *n*-propanol are consistent with those determined for **FR0** in *n*-propanol, indicating that hydrogen bonding with solvent protons plays the same role in both systems. For NCy-**FR0** in DMSO, three rate constants are observed with magnitudes larger than the associated error; these are all associated with direct transitions from the excited electronic state to the ground state ($S_3 \rightarrow S_0$, $S_2 \rightarrow S_0$, $S_1 \rightarrow S_0$) (Table 2). The magnitudes of the rate constants for relaxation between excited states ($S_3 \rightarrow S_2$, $S_3 \rightarrow S_1$, and $S_2 \rightarrow S_1$) are an order of magnitude smaller and in all cases barely larger than their uncertainties. We attribute this finding for DMSO to the absence of excited-state-to-excited-state relaxation in aprotic media. For NCy-**FR0**, hydrogen bonding with the solvent molecules mediates access to relaxation channels between excited states. Most importantly, however, we see similar dynamics in protic media for NCy-**FR0** and **FR0**, reinforcing the assertion that solvent−solute hydrogen bonding interactions proceed predominantly at chromophore carbonyl oxygen, independent of amino nitrogen.

We next investigated the excited-state behavior of MK-**FR0** to determine the effects of substituting the aldehyde proton with a methyl group on **FR0**. To investigate the effects of this substitution on the corresponding excited-state behavior, time-resolved lifetime data were collected for MK-**FR0** in *n*-propanol and DMSO (Figure S4 in the Supporting Information). Consistent with the spectral dynamics of **FR0** and NCy-**FR0**, prominent time-domain spectral dynamics were seen in the experimental data for MK-**FR0** in *n*-propanol (Figure 6a), and the absence of spectral dynamics was observed in DMSO (Figure 6b). It is worth noting that the shift in λ_{max} observed for MK-**FR0** in DMSO compared to NCy-**FR0** in DMSO (Figure 4b) is due to the addition of the methyl group, which alters the electron density distribution of the excited states and the magnitudes of the permanent dipole moments.

Quantum chemical calculations revealed similar excited-state energetics for MK-**FR0** and **FR0**. Similar to **FR0**, the vertical

https://doi.org/10.1021/acs.jpcb.1c06475
J. Phys. Chem. B 2021, 125, 12486−12499

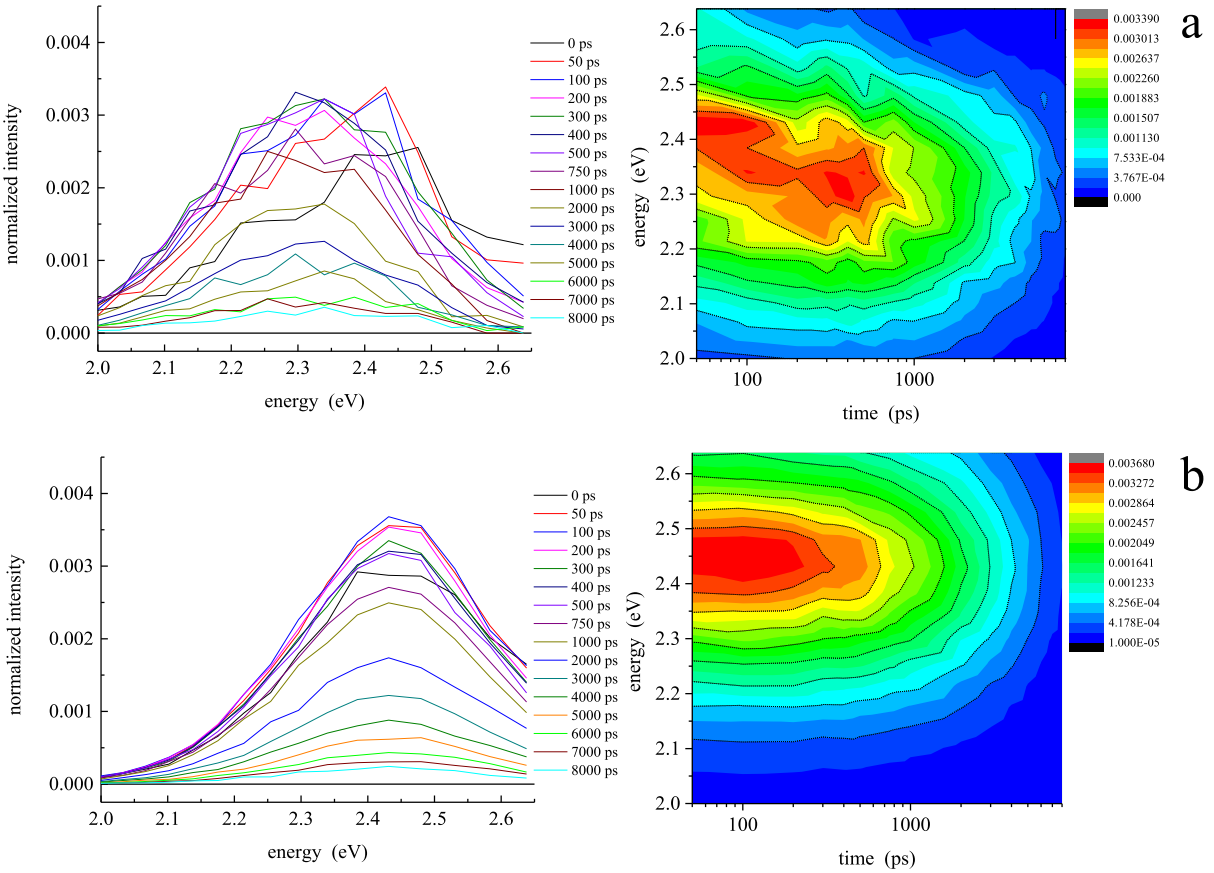

Figure 6. Time-resolved emission spectra for MK-**FR0** in (a) *n*-propanol and (b) DMSO extracted from experimental fluorescence lifetime data. For the spectra in the left panels, the time corresponding to each spectrum is provided in the legends. The right panels are contour plots of the time-resolved spectra.

Table 3. $S_0 \rightarrow S_n$ Vertical Excitation Energies $\omega_n^{(EOMCC)}$ and the Permanent Dipole Moments μ_n Characterizing the Lowest Four Excited Singlet States of MK-FR0 in the Gas Phase[a]

state	$\omega_n^{(EOMCC)}$ (eV)	μ_n (D)
S_1	3.64	13.3
S_2	3.89	1.6
S_3	3.95	9.3
S_4	4.28	4.4

[a]The dipole moment of MK-**FR0** in the ground S_0 state is 5.2 D.

excitation energies for the three lowest excited singlet states of MK-**FR0** are within close energetic proximity, and the permanent dipole moment of the S_2 state is significantly smaller than that characterizing the S_0, S_1, and S_3 states (Table 3). Computational data for the spectroscopic properties (transition dipole moments and oscillator strengths) of MK-**FR0** are similar to those of **FR0** as well and can be found in Table S2 in the Supporting Information. Despite the similarity of the results obtained for MK-**FR0** and **FR0**, small differences in Mulliken charges and the corresponding electron density distributions in the vicinity of the carbonyl moiety have significant consequences, as seen in the experimental time-resolved data. The Mulliken charges and the permanent dipole moment vectors for MK-**FR0** are presented in Figures 7 and 8, respectively.

While the experimental time-resolved spectra indicate the same qualitative role of solvent−solute hydrogen bonding interactions for **FR0** and MK-**FR0** (Figure 6), the Mulliken charges reveal different charge distributions around the carbonyl moiety for **FR0** and MK-**FR0**. The S_2 state plays a solvent-dependent mediating role in intramolecular relaxation dynamics for both chromophores. However, when compared with the Mulliken charges on the aldehyde group in NCy-**FR0** (Figure 2), which are very similar to those obtained for the **FR0** aldehyde group in ref 24, the Mulliken charges on the MK-**FR0** ketone carbon, oxygen, and methyl carbon all differ from those seen for **FR0**. We believe that these differences account for subtle differences in the solvent-dependent trends in the fitted rate constants seen for the two molecules. The carbonyl carbon in the S_0, S_1, and S_3 states is much more positive in MK-**FR0** (Figure 7) than that in NCy-**FR0** (Figure 2), with an effective charge of ca. 0.4. The effective charge decreases to 0.16 in the S_2 state. Consistent with NCy-**FR0**, the charge of the carbonyl oxygen is sufficiently negative in the S_0, S_1, and S_3 states (ca. −0.5) and decreases to −0.17 in the S_2 state. The methyl carbon in MK-**FR0**, however, accumulates a substantial negative charge (ca. −0.8) in all states, which affects the local dipole moment of the methyl ketone moiety. Given the effective charges for these atoms in the S_0, S_1, and S_3 states, the net dipole moment would fall along the axis of the bond between the carbonyl carbon and ring carbon. However, in the S_2 state, there is a comparatively smaller dipole moment between the carbonyl carbon and oxygen, contrasted by a much larger local dipole moment between the carbonyl carbon and methyl carbon. Thus, the net dipole moment of the ketone group would lie along the bond between the carbonyl and

https://doi.org/10.1021/acs.jpcb.1c06475
J. Phys. Chem. B 2021, 125, 12486−12499

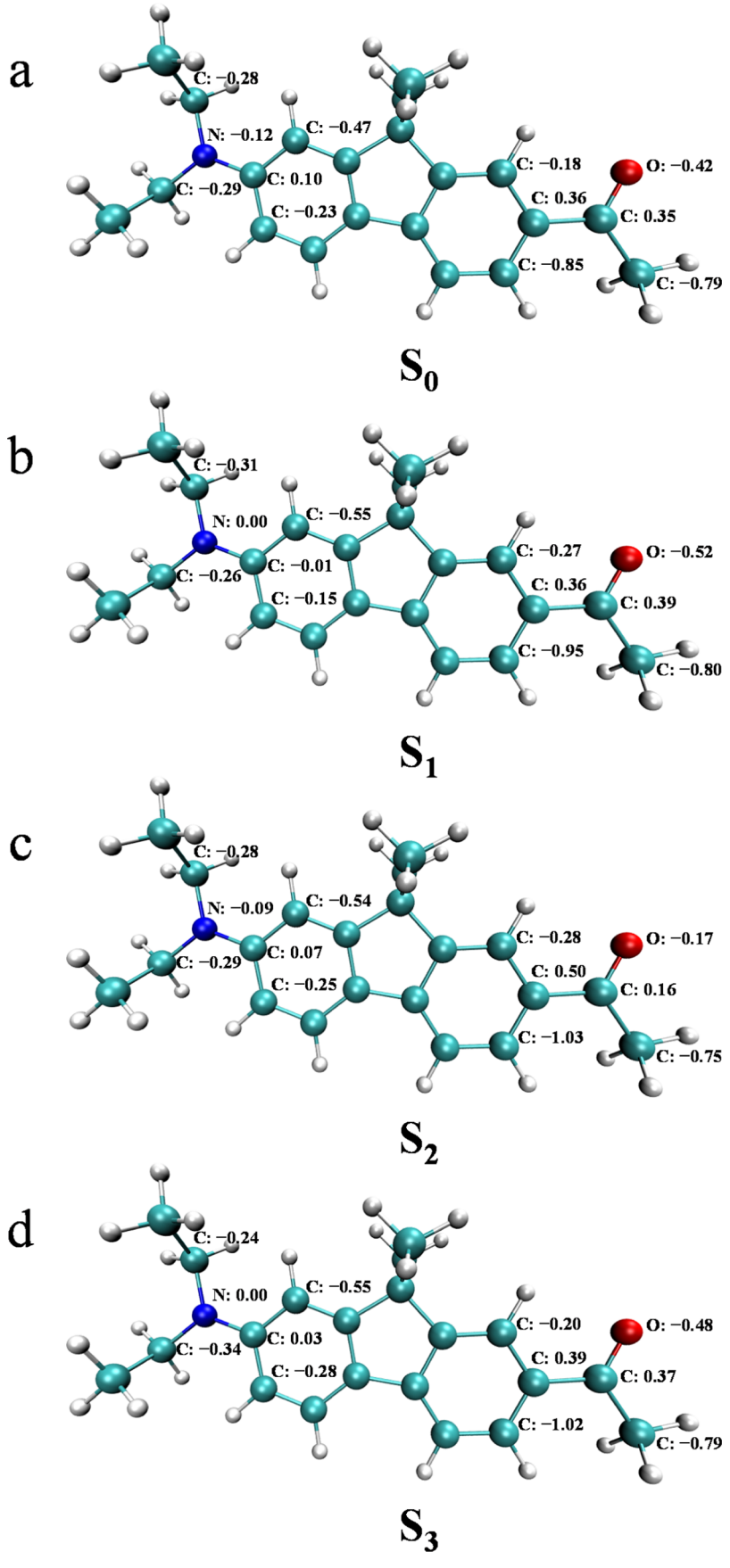

Figure 7. Structure of the isolated MK-**FR0** chromophore in its ground electronic S_0 state and the computed Mulliken charges for selected atoms in (a) S_0, (b) S_1, (c) S_2, and (d) S_3 states of MK-**FR0**.

https://doi.org/10.1021/acs.jpcb.1c06475
J. Phys. Chem. B 2021, 125, 12486−12499

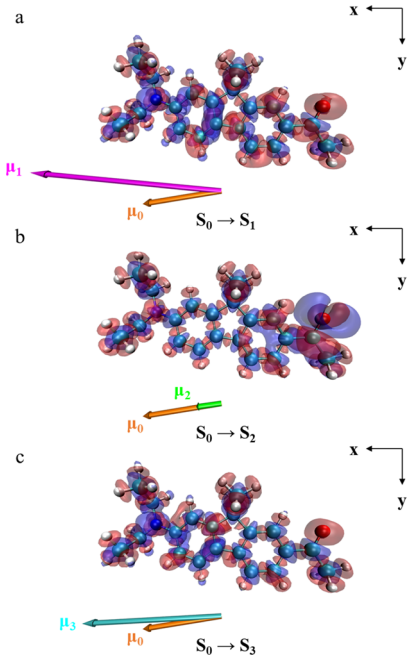

Figure 8. Structure of the isolated MK-**FR0** molecule in its ground electronic S_0 state and the electronic density difference maps associated with the vertical transitions from S_0 to (a) S_1, (b) S_2, and (c) S_3 states of MK-**FR0**. The red/blue color indicates an increase/decrease in electron density upon the $S_0 \rightarrow S_n$ (n = 1−3) excitation, respectively. The dipole moment vectors characterizing the S_0 (orange), S_1 (magenta), S_2 (green), and S_3 (cyan) states of MK-**FR0** are shown as well.

methyl carbon atoms. In the aldehyde group in NCy-**FR0** and **FR0**, the carbonyl carbon is sufficiently more negative in the S_2 state (ca. −0.3 effective charge; Figure 2), giving rise to a net local dipole moment in a different direction from that in MK-**FR0**, which would in turn affect the nature of hydrogen bonding.

To assess the effects of hydroxyl group concentration ([OH]) on the relaxation dynamics of MK-**FR0**, time-resolved spectra were acquired for MK-**FR0** in binary *n*-propanol and DMSO solvent systems, as was performed for **FR0** in ref 24. The individual time-resolved spectra and the corresponding time-domain lifetime data from which the spectra were extracted are presented in Figures S5 and S6 in the Supporting Information. The positions of the unresolved bands within the broad steady-state spectrum of MK-**FR0** in each solvent system were fitted (Figure S7 in the Supporting Information), and the corresponding intensities were extracted to generate the time evolution of each band (Figure 9). The rate constants corresponding to each band decay were fitted using the previously developed kinetic model, and the fitted rate constants are reported in Table 4.

As seen for **FR0**, there is a [OH] dependence for several of the rate constants for MK-**FR0**, particularly for the transitions from the S_3 state (Table 4). The solvent-dependent trends for MK-**FR0** are opposite to those reported for **FR0** in the binary solvent system, as k_{32}, k_{31}, and k_{30} increase with increasing [OH]. This is likely an indication of facile interstate relaxation to the S_2 state, at which point the kinetics are slowed. This is supported by a sufficient decrease in rate constants observed for the transitions associated with the S_2 state (k_{21} and k_{20}), demonstrating the modulating effect of this state on the relaxation dynamics of MK-**FR0**.

Based on these results, it appears that hydrogen bonding interactions of the chromophore carbonyl oxygen with solvent hydroxyl protons still play a central role in determining the spectral dynamics of MK-**FR0**, but the details of the relevant solvent−solute interactions are likely different from those for NCy-**FR0** and **FR0**, which are both aldehydes. The interactions between the carbonyl oxygen and solvent proton create an associated local dipole moment, which will interact with the local dipole moments of the chromophore carbonyl functionalities. As discussed above, the local dipole moments for the ketone and aldehyde for MK-**FR0** and **FR0**, respectively, are oriented differently. While hydrogen bonding interactions still occur for MK-**FR0** at the carbonyl oxygen, the nature of this interaction will be altered by the difference in the local dipole moments of the MK-**FR0** methyl group compared to the **FR0** aldehyde proton. As such, the R−O−H···O═C solvent−solute interaction may align in a spatially different orientation compared to that for **FR0**. This hypothesis will be the focus of future work currently underway as part of this collaborative effort. Based on the data we have presented in this work, hydrogen bonding interactions in the S_2 remain the mediating factor in the excited-state behavior of **FR0** structural precursors, indicating that the spectral dynamics are structurally invariant. However, as demonstrated with MK-**FR0**, while hydrogen bonding mediates relaxation, the nature of the hydrogen bonds is directly related to the functionalities surrounding the **FR0** carbonyl group.

CONCLUSIONS

We have reported on the excited-state behavior and spectral dynamics of two structural precursors to the **FR0** molecule, NCy-**FR0** and MK-**FR0**. Through the use of quantum chemical calculations in concert with experimental data, we have determined that solvent−solute hydrogen bonding interactions still occur upon structural modification to either pendent functionality on the **FR0** core structure. The effect of amino group rotation on the spectral relaxation dynamics was determined to be negligible, as the spectral dynamics, Mulliken charges, and permanent dipole moments for NCy-**FR0** agreed well with those characterizing **FR0**. The ketone analogue MK-**FR0** exhibited similar spectral relaxation dynamics to **FR0** in protic solvents, although subtle differences are observed for the aldehyde and the ketone, and these differences are thought to result from differences in the local charge density distributions seen for the aldehyde and ketone functionalities. These differences give rise to changes in the details of the optimum solvent−solute hydrogen bonding configuration. Despite this difference, both structural precursors were determined to exhibit spectral dynamics similar to those of **FR0**, demonstrating the effect of solvent−solute interactions, particularly those in the S_2 excited state, as the mediators in molecular relaxation dynamics.

It is useful to consider how these results relate to the superphotobase properties of **FR0**-SB. While this connection remains to be made directly, what is clear is that relaxation of population between excited electronic states that characterize the fluorene chromophore depends sensitively on their local environment and on the presence or absence of species capable of hydrogen bonding. From our earlier work on **FR0**-SB, it is clear that the reaction coordinate for proton abstraction from the solvent is dependent on the mode of

https://doi.org/10.1021/acs.jpcb.1c06475
J. Phys. Chem. B 2021, 125, 12486−12499

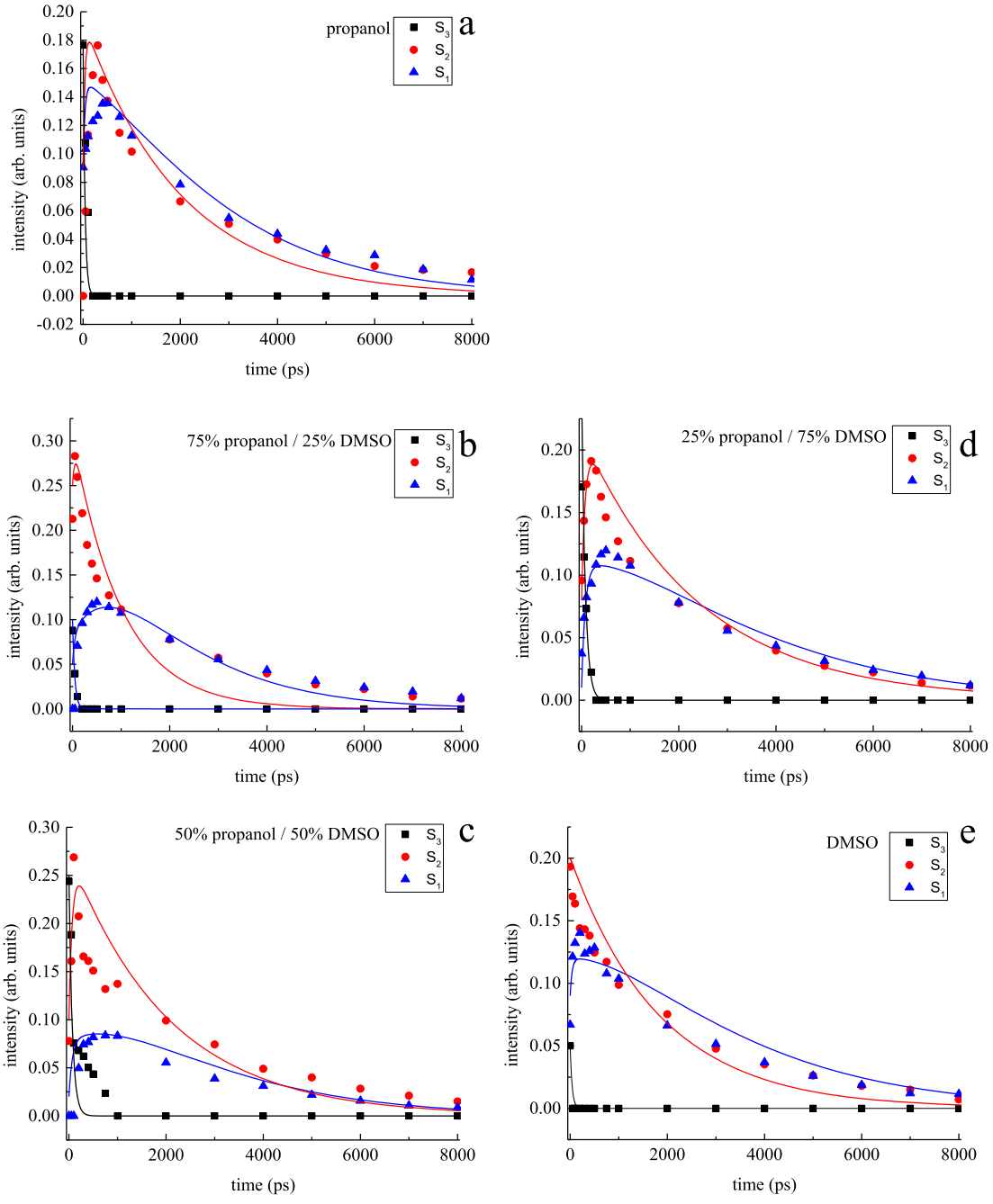

Figure 9. Time-dependent band intensities for three fitted emission bands for MK-**FR0** in (a) *n*-propanol, (b) 75% *n*-propanol/25% DMSO, (c) 50% *n*-propanol/50% DMSO, (d) 25% *n*-propanol/75% DMSO, and (e) DMSO. The data are fitted to the kinetic model using the rate constants in Table 4.

Table 4. Fitted Rate Constants for the Relaxations Associated with Each of the Three Fitted Emission Bands (Spectral Features) for MK-FR0 in *n*-Propanol, DMSO, and Binary Solvent Systems of Increasing *n*-Propanol Concentration in DMSO

	solvent				
rate constant (Hz)	*n*-propanol ($\times 10^9$)	75% *n*-propanol ($\times 10^9$)	50% *n*-propanol ($\times 10^9$)	25% *n*-propanol ($\times 10^9$)	DMSO ($\times 10^9$)
k_{32}	14.76 ± 0.42	11.78 ± 3.16	9.69 ± 0.65	6.91 ± 0.34	0.24 ± 0.25
k_{31}	8.94 ± 0.34	7.54 ± 1.22	3.44 ± 0.59	5.19 ± 0.59	14.58 ± 0.85
k_{30}	2.26 ± 0.47	2.14 ± 0.38	1.25 ± 0.63	1.16 ± 0.48	9.92 ± 0.58
k_{21}	0.39 ± 0.09	0.49 ± 0.14	0.27 ± 0.12	0.28 ± 0.07	0.28 ± 0.11
k_{20}	0.11 ± 0.07	0.51± 0.14	0.22 ± 0.14	0.14 ± 0.07	0.26 ± 0.10
k_{10}	0.66 ± 0.11	0.64 ± 0.16	0.65 ± 0.27	0.53 ± 0.10	0.46 ± 0.10

https://doi.org/10.1021/acs.jpcb.1c06475
J. Phys. Chem. B 2021, 125, 12486−12499

excitation,[60] with the clear implication that the relaxation pathway within the chromophore, which involves multiple excited electronic states, is of central importance to the photobase behavior of the imine nitrogen Schiff base in **FR0**-SB. In the structural precursors reported here and in ref 24, the intramolecular relaxation dynamics also influence the electron density distribution in the same relative position on the fluorene ring system, indicating that solvent interactions with the chromophores mediate the intramolecular relaxation dynamics. It is thus not simply the imine functionality of **FR0**-SB that gives rise to its super-photobase behavior. The electronic structure and intramolecular relaxation dynamics of the fluorene derivative chromophore play an important role in the photobase properties of **FR0**-SB.

■ ASSOCIATED CONTENT

Supporting Information

The Supporting Information is available free of charge at https://pubs.acs.org/doi/10.1021/acs.jpcb.1c06475.

Calculated transition dipole moments and oscillator strengths, time-resolved intensity data, steady-state absorption and emission spectra, fits of steady-state emission spectra to three Gaussian functions, kinetic model, and time-resolved spectra for mixed propanol−DMSO solvent systems (PDF)

■ AUTHOR INFORMATION

Corresponding Author

G. J. Blanchard − *Department of Chemistry, Michigan State University, East Lansing, Michigan 48824, United States;* orcid.org/0000-0002-1207-0810; Phone: +1 517 353 1105; Email: blanchard@chemistry.msu.edu

Authors

Briana A. Capistran − *Department of Chemistry, Michigan State University, East Lansing, Michigan 48824, United States*

Stephen H. Yuwono − *Department of Chemistry, Michigan State University, East Lansing, Michigan 48824, United States;* orcid.org/0000-0002-6604-3543

Mehdi Moemeni − *Department of Chemistry, Michigan State University, East Lansing, Michigan 48824, United States*

Soham Maity − *Department of Chemistry, Michigan State University, East Lansing, Michigan 48824, United States*

Aria Vahdani − *Department of Chemistry, Michigan State University, East Lansing, Michigan 48824, United States*

Babak Borhan − *Department of Chemistry, Michigan State University, East Lansing, Michigan 48824, United States;* orcid.org/0000-0002-3193-0732

James E. Jackson − *Department of Chemistry, Michigan State University, East Lansing, Michigan 48824, United States;* orcid.org/0000-0002-4506-7415

Piotr Piecuch − *Department of Chemistry, Michigan State University, East Lansing, Michigan 48824, United States; Department of Physics and Astronomy, Michigan State University, East Lansing, Michigan 48824, United States;* orcid.org/0000-0002-7207-1815

Marcos Dantus − *Department of Chemistry, Michigan State University, East Lansing, Michigan 48824, United States; Department of Physics and Astronomy, Michigan State University, East Lansing, Michigan 48824, United States;* orcid.org/0000-0003-4151-5441

Complete contact information is available at: https://pubs.acs.org/10.1021/acs.jpcb.1c06475

Notes

The authors declare no competing financial interest.

■ ACKNOWLEDGMENTS

This work was funded by a seed grant from DARPA and AMRDEC (W31P4Q-20-1-0001). Partial support comes from the NIH (grant nos. 2R01EY016077-08A1 and 5R01EY025383-02 R01 to G.J.B. and R01GM101353 to B.B.), the NSF (grant no. CHE1836498 to M.D.), and the U.S. DOE (grant no. DE-FG02-01ER15228 to P.P.). This work was supported in part through computational resources and services provided by the Institute for Cyber-Enabled Research at Michigan State University. The views and conclusions contained in this document are those of the authors and should not be interpreted as representing the official policies, either expressed or implied, of the Defense Advanced Research Projects Agency, the U.S. Army, or the U.S. Government. The authors would like to thank Dr. Ilias Magoulas for providing the code used in generating the electronic density difference maps shown in this work.

■ REFERENCES

(1) Agmon, N.; Rettig, W.; Groth, C. Electronic Determinants of Photoacidity in Cyanonaphthols. *J. Am. Chem. Soc.* **2002**, *124*, 1089−1096.

(2) Barroso, M.; Arnaut, L. G.; Formosinho, S. J. Intersecting State Model Calculations on Fast and Ultrafast Excited State Proton Transfers in Naphthols and Substituted Naphthols. *J. Photochem. Photobiol., A* **2002**, *154*, 13−21.

(3) Clower, C.; Solntsev, K. M.; Kowalik, J.; Tolbert, L. M.; Huppert, D. Photochemistry of "Super" Photoacids. 3. Excited State Proton Transfer from Perfluoroalkylsulfonyl-Substituted 2-Naphthols. *J. Phys. Chem. A* **2002**, *106*, 3114−3122.

(4) Cohen, B.; Huppert, D. Unusual Temperature Dependence of Excited State Proton Transfer Rates in Alcohols. *J. Phys. Chem. A* **2000**, *104*, 2663−2667.

(5) Cohen, B.; Segal, J.; Huppert, D. Proton Transfer from Photoacid to Solvent. *J. Phys. Chem. A* **2002**, *106*, 7462−7467.

(6) Finkler, B.; Spies, C.; Vester, M.; Walte, F.; Omlor, K.; Riemann, I.; Zimmer, M.; Stracke, F.; Gerhards, M.; Jung, G. Highly Photostable "Super"-Photoacids for Ultrasensitive Fluorescence Spectroscopy. *Photochem. Photobiol. Sci.* **2014**, *13*, 548−562.

(7) Huppert, D.; Tolbert, L. M.; Linares-Samaniego, S. Ultrafast Excited State Proton Transfer from Cyano-Substituted 2-Naphthols. *J. Phys. Chem. A* **1997**, *101*, 4602−4605.

(8) Knochenmuss, R.; Solntsev, K. M.; Tolbert, L. M. Molecular Beam Studies of the "Super" Photoacid 5-Cyano-2-Naphthol in Solvent Clusters. *J. Phys. Chem. A* **2001**, *105*, 6393−6401.

(9) Malval, J.-P.; Diemer, V.; Savary, F. M.; Jacques, P.; Allonas, X.; Chaumeil, H.; Defoin, A.; Carré, C. Excited State Proton Transfer in a "Super" Photoacid based on a Phenol−Pyridinium Biaryl Chromophore. *Chem. Phys. Lett.* **2008**, *455*, 238−241.

(10) Schulman, S. G. Acid Base Chemistry of Excited Singlet States. In *Modern Fluorescence Spectroscopy*; Wehry, E. L., Ed.; Plenum Press: New York, 1976; pp 239−275.

(11) Solntsev, K. M.; Huppert, D.; Agmon, N. Photochemistry of "Super" Photoacids. Solvent Effects. *J. Phys. Chem. A* **1999**, *103*, 6984−6997.

(12) Solntsev, K. M.; Huppert, D.; Agmon, N.; Tolbert, L. M. Photochemistry of "Super" Photoacids. 2. Excited State Proton Transfer in Methanol/Water Mixtures. *J. Phys. Chem. A* **2000**, *104*, 4658−4669.

(13) Solntsev, K. M.; Huppert, D.; Tolbert, L. M.; Agmon, N. Solvatochromic Shifts of "Super" Photoacids. *J. Am. Chem. Soc.* **1998**, *120*, 7981−7982.
(14) Solntsev, K. M.; Tolbert, L. M.; Cohen, B.; Huppert, D.; Hayashi, Y.; Feldman, Y. Excited State Proton Transfer in Chiral Environments. 1. Chiral Solvents. *J. Am. Chem. Soc.* **2002**, *124*, 9046−9047.
(15) Tolbert, L. M.; Haubrich, J. E. Enhanced Photoacidities of Cyanonaphthols. *J. Am. Chem. Soc.* **1990**, *112*, 8163−8165.
(16) Tolbert, L. M.; Haubrich, J. E. Photoexcited Proton Transfer from Enhanced Photoacids. *J. Am. Chem. Soc.* **1994**, *116*, 10593−10600.
(17) Tolbert, L. M.; Solntsev, K. M. Excited State Proton Transfer: From Constrained Systems to "Super" Photoacids to Superfast Proton Transfer. *Acc. Chem. Res.* **2002**, *35*, 19−27.
(18) Lahiri, J.; Moemeni, M.; Kline, J.; Borhan, B.; Magoulas, I.; Yuwono, S. H.; Piecuch, P.; Jackson, J. E.; Dantus, M.; Blanchard, G. J. Proton Abstraction Mediates Interactions between the Super Photobase FR0-SB and Surrounding Alcohol Solvent. *J. Phys. Chem. B* **2019**, *123*, 8448−8456.
(19) Lahiri, J.; Moemeni, M.; Kline, J.; Magoulas, I.; Yuwono, S. H.; Laboe, M.; Shen, J.; Borhan, B.; Piecuch, P.; Jackson, J. E.; et al. Isoenergetic Two-Photon Excitation Enhances Solvent-to-Solute Excited-State Proton Transfer. *J. Chem. Phys.* **2020**, *153*, 224301.
(20) Lahiri, J.; Moemeni, M.; Magoulas, I.; Yuwono, S. H.; Kline, J.; Borhan, B.; Piecuch, P.; Jackson, J. E.; Blanchard, G. J.; Dantus, M. Steric Effects in Light-Induced Solvent Proton Abstraction. *Phys. Chem. Chem. Phys.* **2020**, *22*, 19613−19622.
(21) Sheng, W.; Nairat, M.; Pawlaczyk, P. D.; Mroczka, E.; Farris, B.; Pines, E.; Geiger, J. H.; Borhan, B.; Dantus, M. Ultrafast Dynamics of a "Super" Photobase. *Angew. Chem., Int. Ed. Engl.* **2018**, *57*, 14742−14746.
(22) Hunt, J. R.; Dawlaty, J. M. Photodriven Deprotonation of Alcohols by a Quinoline Photobase. *J. Phys. Chem. A* **2018**, *122*, 7931−7940.
(23) Hunt, J. R.; Dawlaty, J. M. Kinetic Evidence for the NEcessity of Two Proton Donor Molecules for Successful Excited State Proton Transfer by a Photobase. *J. Phys. Chem. A* **2019**, *123*, 10372−10380.
(24) Capistran, B. A.; Yuwono, S. H.; Moemeni, M.; Maity, S.; Vahdani, A.; Borhan, B.; Jackson, J. E.; Piecuch, P.; Dantus, M.; Blanchard, G. J. Excited State Dynamics of a Substituted Fluorene Derivative. The Central Role of Hydrogen Bonding Interactions with the Solvent. *J. Phys. Chem. B* **2021**, DOI: 10.1021/acs.jpcb.1c06474. in press
(25) Kucherak, O. A.; Didier, P.; Mély, Y.; Klymchenko, A. S. Fluorene Analogues of Prodan with Superior Fluorescence Brightness and Solvatochromism. *J. Phys. Chem. Lett.* **2010**, *1*, 616−620.
(26) Pillman, H. A.; Blanchard, G. J. Effects of Energy Dissipation on Motional Dynamics in Unilamellar Vesicles. *J. Phys. Chem. B* **2010**, *114*, 13703−13709.
(27) Stanton, J. F.; Bartlett, R. J. The Equation of Motion Coupled-Cluster Method. A Systematic Biorthogonal Approach to Molecular Excitation Energies, Transition Probabilities, and Excited State Properties. *J. Chem. Phys.* **1993**, *98*, 7029−7039.
(28) Clark, T.; Chandrasekhar, J.; Spitznagel, G. n. W.; Schleyer, P. v. R. Efficient Diffuse Function-Augmented Basis Sets for Anion Calculations. III. The 3-21+G Basis Set for First-Row Elements, Li−F. *J. Comp. Chem.* **1983**, *4*, 294−301.
(29) Hariharan, P. C.; Pople, J. A. The Influence of Polarization Functions on Molecular Orbital Hydrogenation Energies. *Theor. Chim. Acta* **1973**, *28*, 213−222.
(30) Hehre, W. J.; Ditchfield, R.; Pople, J. A. Self-Consistent Molecular Orbital Methods. XII. Further Extensions of Gaussian-Type Basis Sets for use in Molecular Orbital Studies of Organic Molecules. *J. Chem. Phys.* **1972**, *56*, 2257−2261.
(31) Fradelos, G.; Lutz, J. J.; Wesołowski, T. A.; Piecuch, P.; Włoch, M. Embedding vs. Supermolecular Strategies in Evaluating the Hydrogen-Bonding-Induced Shifts of Excitation Energies. *J. Chem. Theory Comput.* **2011**, *7*, 1647−1666.
(32) Piecuch, P.; Gour, J. R.; Włoch, M. Left-Eigenstate Completely Renormalized Equation-of-Motion Coupled-Cluster Methods: Review of Key Concepts, Extension to Excited States of Open-Shell Systems, and Comparison with Electron-Attached and Ionized Approaches. *Int. J. Quantum Chem.* **2009**, *109*, 3268−3304.
(33) Łoch, M. W.; Lodriguito, M. D.; Piecuch, P.; Gour, J. R. Two New Classes of Non-Iterative Coupled-Cluster Methods Derived from the Method of Moments of Coupled-Cluster Equations. *Mol. Phys.* **2006**, *104*, 2149−2172.
(34) Barca, G. M. J.; Bertoni, C.; Carrington, L.; Datta, D.; De Silva, N.; Deustua, J. E.; Fedorov, D. G.; Gour, J. R.; Gunina, A. O.; Guidez, E.; et al. Recent Developments in the General Atomic and Molecular Electronic Structure System. *J. Chem. Phys.* **2020**, *152*, 154102.
(35) Gordon, M. S.; Schmidt, M. W. Advances in Electronic Structure Theory: GAMESS a Decade Later. In *Theory and Applications of Computational Chemistry: The First Forty Years*; Dykstra, C. E., Frenking, G., Kim, K. S., Scuseria, G. E., Eds.; Elsevier: Amsterdam, 2005; pp 1167−1189.
(36) Bagchi, B.; Oxtoby, D. W.; Fleming, G. R. Theory of the Time Development of the Stokes Shift in Polar Media. *Chem. Phys.* **1984**, *86*, 257−267.
(37) Castner, E. W., Jr.; Fleming, G. R.; Bagchi, B. Influence of non-Debye Relaxation and of Molecular Shape on the Time Dependence of the Stokes Shift in Polar Media. *Chem. Phys. Lett.* **1988**, *143*, 270−276.
(38) Castner, E. W., Jr.; Maroncelli, M.; Fleming, G. R. Subpicosecond Resolution Studies of Solvation Dynamics in Polar Aprotic and Alcohol Solvents. *J. Chem. Phys.* **1987**, *86*, 1090−1097.
(39) Eom, I.; Joo, T. Polar Solvation Dynamics of Coumarin 153 by Ultrafast Time-Resolved Fluorescence. *J. Chem. Phys.* **2009**, *131*, 244507.
(40) Maroncelli, M.; Fleming, G. R. Picosecond Solvation Dynamics of Coumarin 153: The Importance of Molecular Aspects of Solvation. *J. Chem. Phys.* **1987**, *86*, 6221−6239.
(41) Maroncelli, M.; Fleming, G. R. Comparison of Time-Resolved Fluorescence Stokes Shift Measurements to a Molecular Theory of Solvation Dynamics. *J. Chem. Phys.* **1988**, *89*, 875−881.
(42) Nagarajan, V.; Brearley, A. M.; Kang, T. J.; Barbara, P. F. Time-Resolved Spectroscopic Measurements on Microscopic Solvation Dynamics. *J. Chem. Phys.* **1987**, *86*, 3183−3196.
(43) Simon, J. D.; Su, S.-G. Picosecond Stokes Shift Studies of Solvent Friction: Experimental Measurements of Time-Dependent Band Shape and Integrated Intensity. *Chem. Phys.* **1991**, *152*, 143−152.
(44) Su, S. G.; Simon, J. D. Solvation Dynamics in Ethanol. *J. Phys. Chem.* **1987**, *91*, 2693−2696.
(45) Adhikary, R.; Barnes, C. A.; Petrich, J. W. Solvation Dynamics of the Fluorescent Probe PRODAN in Heterogeneous Environments: Contributions from the Locally Excited and Charge-Transferred States. *J. Phys. Chem. B* **2009**, *113*, 11999−12004.
(46) Agmon, N. Dynamic Stokes Shift in Coumarin: Is it Only Relaxation? *J. Phys. Chem.* **1990**, *94*, 2959−2963.
(47) Blanchard, G. J. Time-Resolved Measurement of the Stimulated Emission Stokes Shift in LDS750: Evidence for Inhomogeneous Relaxation Kinetics. *J. Chem. Phys.* **1991**, *95*, 6317−6325.
(48) Hébert, P.; Baldacchino, G.; Gustavsson, T.; Mialocq, J.-C. Sub-Picosecond Fluorescence Study of the LDS 751 Dye Molecule in Ethanol. *Chem. Phys. Lett.* **1993**, *213*, 345−350.
(49) Hermant, R. M.; Bakker, N. A. C.; Scherer, T.; Krijnen, B.; Verhoeven, J. W. Systematic study of a Series of Highly Fluorescent Rod-Shaped Donor-Acceptor Systems. *J. Am. Chem. Soc.* **1990**, *112*, 1214−1221.
(50) Jiang, Y.; McCarthy, P. K.; Blanchard, G. J. The Role of Multiple Electronic States in the Dissipative Energy Dynamics of Coumarin 153. *Chem. Phys.* **1994**, *183*, 249−267.
(51) McCarthy, P. K.; Blanchard, G. J. AM1 Study of the Electronic Structure of Coumarins. *J. Phys. Chem.* **1993**, *97*, 12205−12209.

(52) Middelhoek, E. R.; van der Meulen, P.; Verhoeven, J. W.; Glasbeek, M. Picosecond Time-Dependent Stokes Shift Studies of Fluoroprobe in Liquid Solution. *Chem. Phys.* **1995**, *198*, 373−380.
(53) Middelhoek, E. R.; Zhang, H.; Verhoeven, J. W.; Glasbeek, M. Subpicosecond Studies of the Solvation Dynamics of Fluoroprobe in Liquid Solution. *Chem. Phys.* **1996**, *211*, 489−497.
(54) Silori, Y.; Dey, S.; De, A. K. How to Study Picosecond Solvation Dynamics using Fluorescent Probes with Small Stokes Shifts. *Chem. Phys. Lett.* **2018**, *693*, 222−226.
(55) Eber, G.; Grüneis, F.; Schneider, S.; Dörr, F. Dual Fluorescence Emission of Azulene Derivatives in Solution. *Chem. Phys. Lett.* **1974**, *29*, 397−404.
(56) Huppert, D.; Jortner, J.; Rentzepis, P. M. $S_2 \rightarrow S_1$ Emission of Azulene in Solution. *Chem. Phys. Lett.* **1972**, *13*, 225−228.
(57) Karpovich, D. S.; Blanchard, G. J. Relating the Polarity-Dependent Fluorescence Response of Pyrene to Vibronic Coupling. Achieving a Fundamental Understanding of the py Polarity Scale. *J. Phys. Chem.* **1995**, *99*, 3951−3958.
(58) Orlandi, G.; Siebrand, W. Mechanisms of Vibronic Intensity Borrowing. *Chem. Phys. Lett.* **1972**, *15*, 465−468.
(59) Orlandi, G.; Siebrand, W. Theory of Vibronic Intensity Borrowing. Comparison of Herzberg-Teller and Born-Oppenheimer Coupling. *J. Chem. Phys.* **1973**, *58*, 4513−4523.
(60) Lahiri, J.; Yuwono, S. H.; Magoulas, I.; Moemeni, M.; Borhan, B.; Blanchard, G. J.; Piecuch, P.; Dantus, M. Controlling Quantum Interference between Virtual and Dipole Two-Photon Optical Excitation Pathways Using Phase-Shaped Laser Pulses. *J. Phys. Chem. A* **2021**, *125*, 7534−7544.

https://doi.org/10.1021/acs.jpcb.1c06475
J. Phys. Chem. B 2021, 125, 12486−12499